Elucidation of the orbital moment, anisotropy and magnetic damping in epitaxial Fe_3O_4

C. Love[1,2], J. E. Beevers[1], B. Achinuq[1], R. Fan[2], K. Matsuzaki[3], T. Susaki[4,5], V. K. Lazarov[1], S. S. Dhesi[2], G. van der Laan[2] and S. A. Cavill[1,2*]

[1]Department of Physics, University of York, York YO10 5DD, UK
[2]Diamond Light Source, Harwell Science and Innovation Campus, Didcot, OX11 0DE, UK
[3]Research Institute for Advanced Electronics and Photonics, National Institute of Advanced Industrial Science and Technology, Tsukuba, Ibaraki, 305-8568 Japan
[4]Science & Innovation Center, Mitsubishi Chemical Corporation 1000 Kamoshida-cho, Aoba-ku, Yokohama-shi, Kanagawa 227-8502, Japan
[5]Secure Materials Center, Materials and Structures Laboratory, Tokyo Institute of Technology, 4259 Nagatsuta, Midori-ku, Yokohama 226-8503, Japan

*email: stuart.cavill@york.ac.uk

Abstract

The size of the orbital moment in Fe_3O_4 has provided a long standing and contentious debate. In this paper we make use of ferromagnetic resonance (FMR) spectroscopy and x-ray magnetic circular dichroism (XMCD) to provide complementary determinations of the size of the orbital moment in "bulk-like" epitaxial Fe_3O_4 films grown on Yttria-stabilized zirconia (111) substrates. Annealing the 100 nm as-grown films to 1100 °C in a reducing atmosphere improves the stoichiometry and microstructure of the films allowing for bulk like properties to be recovered as evidenced by X-ray diffraction (XRD) and vibrating sample magnetometry (VSM). In addition, in-plane angular FMR spectra exhibit a cross over from a 4-fold symmetry to the expected 6-fold symmetry of the (111) surface, together with an anomalous peak in the FMR linewidth at ~10 GHz; indicative of low Gilbert damping in combination with two-magnon scattering. For the bulk-like annealed sample, a spectroscopic splitting factor $g \approx 2.18$ is obtained using both FMR and XMCD techniques, providing evidence for the presence of a finite orbital moment in Fe_3O_4.

Introduction

The interest in half-metal materials which are predicted to be 100% spin polarized at the Fermi level has been a major driver in spintronic research over the past decade [1]. Fe_3O_4 is the archetypal half-metal material due to its predicted 100% polarization at the Fermi level, high Curie temperature (T_C = 858 K) and good epitaxial match to technologically important semiconductors and oxides (e.g., GaAs, MgO, and Al_2O_3), yet the promise of a fully spin polarized Fermi level has not been realised. Achieving a fully ordered high quality Fe_3O_4 thin film is essential for spintronic device applications and a number of studies have been devoted to growth optimization in order to achieve this. However, the problem with thin film magnetite is that it tends to show non-bulk like magnetoresistance (MR) and presents high saturation fields regardless of film growth technique [2]. The difficulty in magnetically saturating these films has been associated with the presence of anti-phase boundaries (APBs) between ferrimagnetic domains. These have been invoked to explain the large negative magnetoresistance observed in Fe_3O_4 [3]. In line with the Goodenough-Kanamori-Anderson rules [4] Fe–O–Fe bond angles close to 180°, induced by APBs, give rise to superexchange interactions coupling the adjacent domains antiferromagnetically. The existence of APBs has been extensively reported in the literature and the anomalous thin film properties correlated to the APB atomic structure and density [5-6]. In order to improve the structural ordering of the Fe_3O_4 thin films and reduce the APB density, post annealing in a CO/CO_2 atmosphere has been successfully employed [7] and shown to correlate with near bulk like magnetotransport properties.

In this paper we demonstrate that CO/CO_2 annealed films recover bulk-like magnetic properties including the expected anisotropy for the (111) geometry. For the annealed sample the magnetic damping is still dominated by two magnon scattering (TMS) which is indicative of magnetic inhomogeneities. In particular, a peak in the linewidth as a function of frequency is observed in the FMR data which has only been previously seen in spherical samples [8] or samples with small intrinsic Gilbert damping in combination with TMS [9]. We show than this non-monotonic behavior is consistent with a small out-of-plane tilting of the magnetization in combination with TMS. Finally, using the two complementary techniques of XMCD and FMR, we unequivocally establish that a finite orbital moment exists in Fe_3O_4.

Methods

Nominally 100 nm Fe_3O_4 films were grown by pulsed laser deposition (PLD) on Yttria-stabilized zirconia (YSZ) substrates at 300°C in a partial oxygen pressure of P_{oxygen} = 2 x10^{-4} Pa. Post annealing was performed on 1 of the films at 1100° C for 60 min in a CO/CO_2 atmosphere with a ratio of 1:5000 as detailed in previous studies [7]. XRD measurements were performed using a non-monochromated Cu $K\alpha$ source whilst the magnetic measurements were performed using a VSM-SQUID and FMR spectrometer [10]. Fe $L_{2,3}$ x-ray absorption spectroscopy (XAS) and XMCD measurements were performed on beamline I06 at the Diamond Light Source [11]. The XAS was measured in normal incidence by total-electron yield (TEY) using the sample drain current.

Results

XRD measurements are shown in Fig. 1 for (a) the as-deposited film and (b) the annealed film. In Fig. 1(a) four peaks are indexed to the (*hkl*) reflections, where $h = k = l$, of the Fe_3O_4 structure (space group *Fd*-3*m*, inverse spinel, $a = b = c$ = 8.396 Å) with a lattice constant of 8.440(3) Å. The other peaks in the data are substrate reflections due to the unmonochromated beam. Surprisingly, the Fe_3O_4 film retains the epitaxial relationship with the YZS(111) substrate with the following crystallographic relationship, YSZ(111) || Fe_3O_4(111) and YSZ(1-10)|| Fe_3O_4(1-10), even though the lattice mismatch is ≈ 22 %, $(|a_{YSZ}/\sqrt{2} - a_{Fe3O4}/2\sqrt{2}|/(a_{Fe3O4}/2\sqrt{2})$; a_{YSZ} = 5.12 Å.

Fig. 1(b) shows the XRD data for the annealed sample. The same family of (*hhh*) peaks are present as in the as-deposited case, retaining the epitaxial relationship to the substrate. However, a clear shift of the reflections to higher angles is seen, giving a smaller lattice constant of 8.355(2) Å compared to the as-deposited case. Upon annealing the Fe_3O_4 goes from being compressively strained in the plane of the sample with respect to bulk Fe_3O_4, to being under tension.

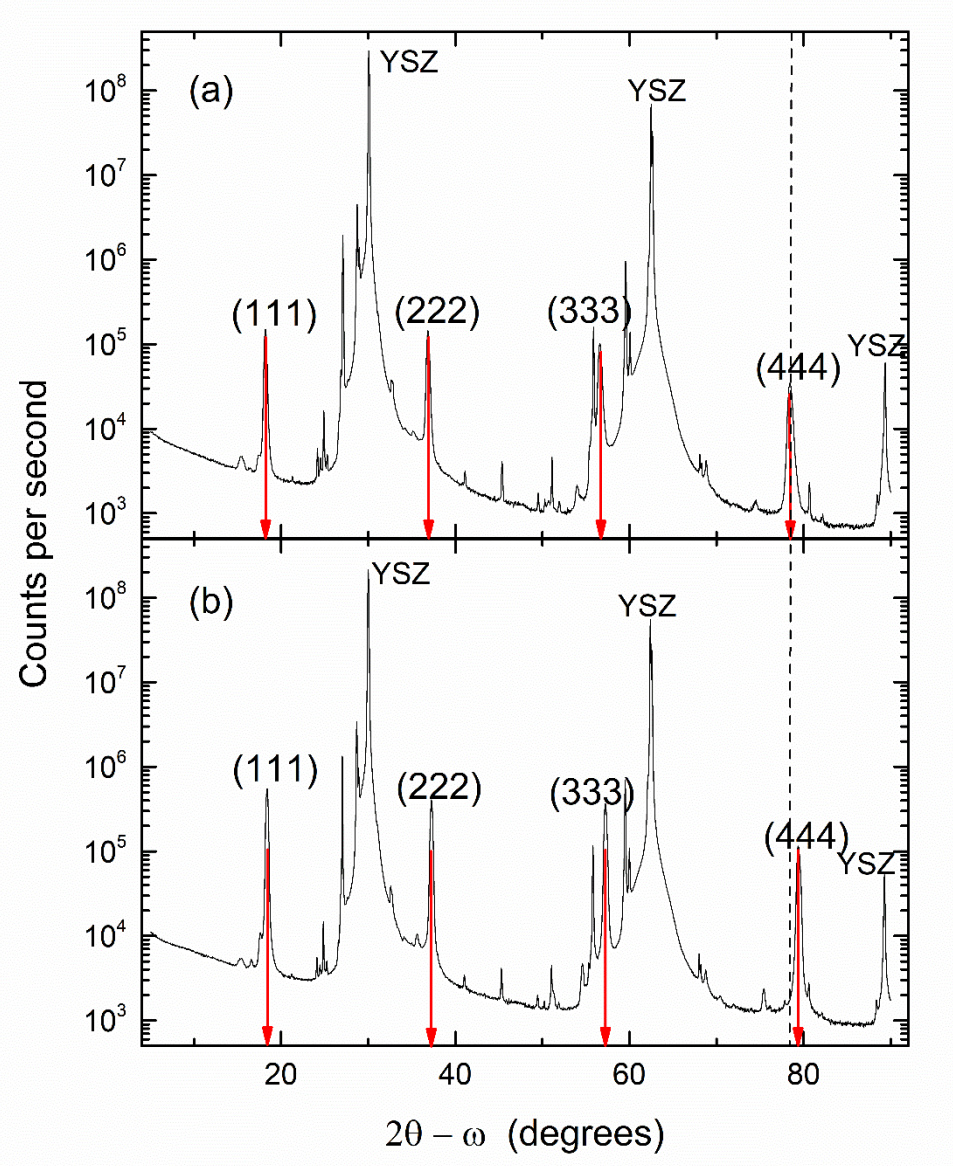

Figure 1: XRD measured in the symmetric geometry for (a) the as-grown sample and (b) the anenaled sample. Red arrows indicate the position of the (hhh) Fe_3O_4 reflections.

VSM measurements were performed with the applied field parallel to the surface along the $[1\bar{2}1]$ direction for temperatures between 5 and 300 K. Fig. 2 shows magnetometry data for the as-grown and annealed films. Room temperature *M*(*H*) data is shown in Figs. 2(a) and 2(c) for the as-grown and the annealed films respectively, whilst the temperature dependent magnetization, after field cooling in a saturating field of 30 kOe, is shown in Figs. 2(b) and 2(d). The effect of annealing in the CO/CO_2 environment is evident from the increase in saturation magnetization from 260 emu/cc to ≈ 470 emu/cc, the decrease in coercivity (580 to 52 Oe) and the increased squareness of the loop (0.3 to 0.8) which all suggest an improved magnetic structure with bulk-like properties. Magnetic structure improvements due to the annealing procedure can also be seen in the field cooled *M*(*T*) data. The as-grown sample magnetization drops rapidly around 100 K before decreasing more gradually at

approximately 120 K. Conversely, the annealed sample displays a sharp increase in magnetization around 115 K before gradually decreasing with temperature. Such behavior is typical of bulk magnetite around the Verwey transition temperature, known to be a very sensitive probe of chemical disorder [12].

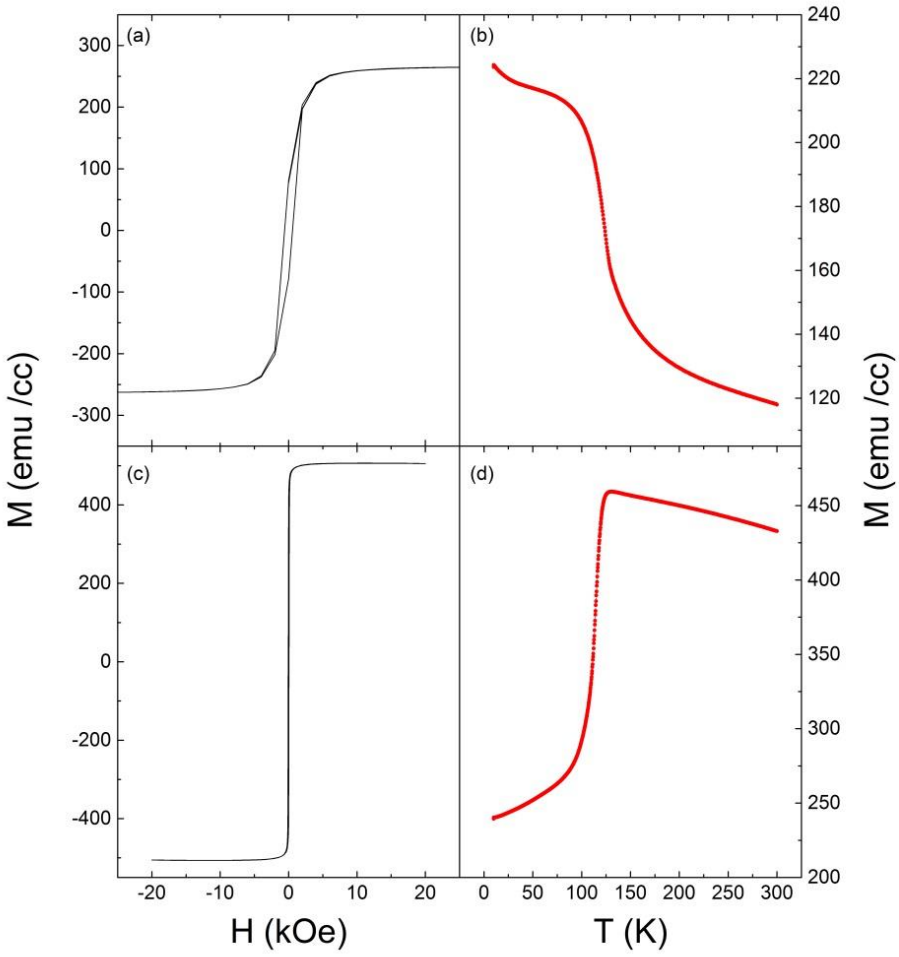

Figure 2: (a) M-H and (b) M-T for the as-grown film. (c) M-H and (d) M-T for the annealed film. M-H curves were measured at 300 K. M-T curves were measured after field cooling at 30 KOe. The measuring field was set to 1000 Oe.

To gain a detailed understanding of the role of CO/CO_2 annealed Fe_3O_4, XAS / XMCD measurements were performed at the Fe $L_{2,3}$ absorption edges in order to determine valency, coordination, and magnetic properties of the Fe cations. In *L*-edge XAS, electrons are excited from a 2*p* core level to the unoccupied 3*d* valence states of the element of interest by circularly polarized x-rays at the resonance energy of the transition. The difference in absorption for opposite chirality of the polarizations (XMCD) gives a direct and element-specific measurement of the projection of the 3*d* magnetic moment along the x-ray helicity vector [13]. The absorption cross section is commonly obtained by measuring the decay products, typically total-electron yield (TEY) detection, of the photo-excited core hole. The type of decay product measured determines the probing depth of the technique. At the $L_{2,3}$ absorption edges of 3*d* transition metals the probing depth for TEY detection is approximately 6 nm. All

measurements were performed at normal incidence, which reduces the effect of self-absorption on the spectra [14], in a 5 T field applied collinear to the x-ray helicity vector.

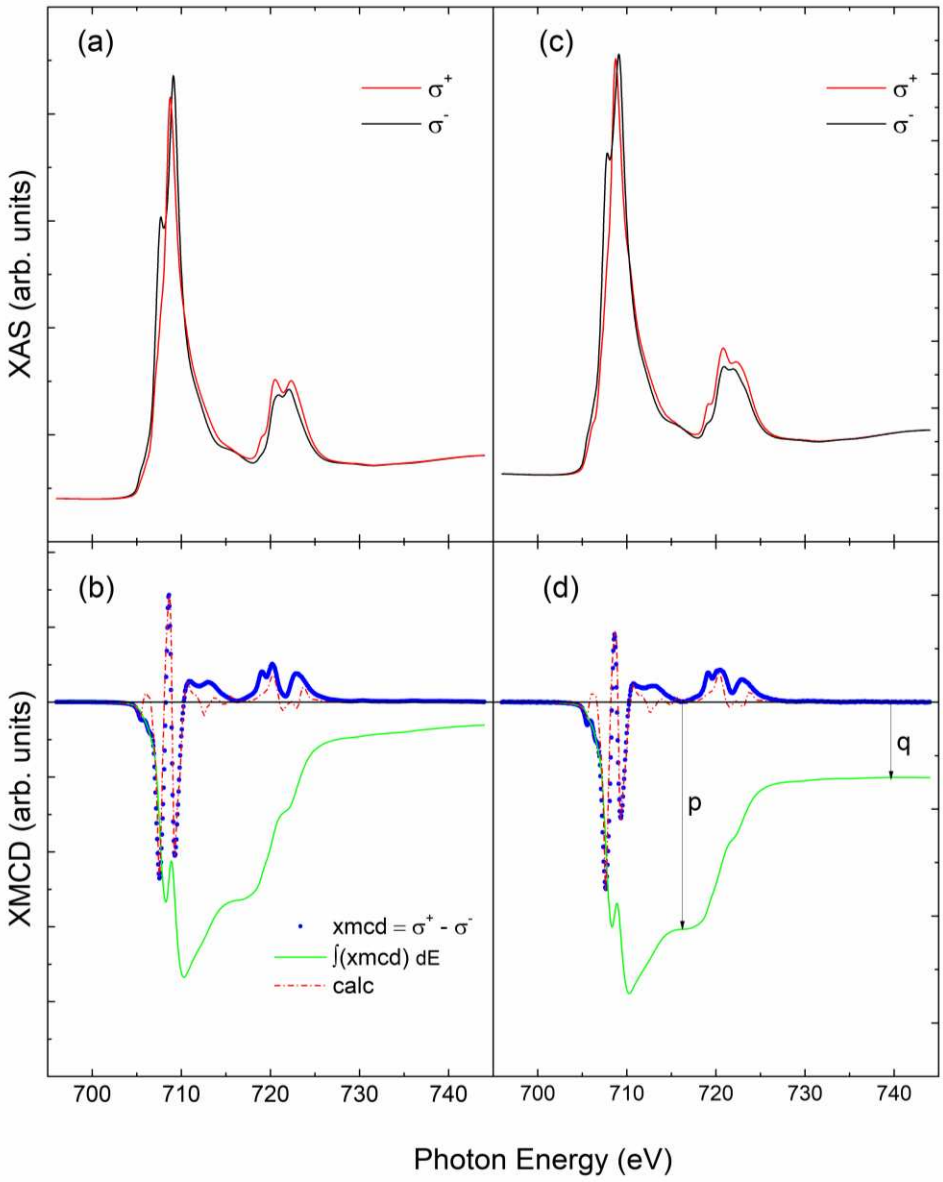

Figure 3. Circular polarization dependent XAS at the Fe $L_{2,3}$ edges for (a) the as-grown sample and (c) the annealed sample. XMCD (blue dots) and integrated XMCD (green line) specta for (b) the as-grown sample and (d) the annealed sample. Atomic multiplet simulations of the XMCD are shown in red dash-dot line on top of the experimental XMCD. p is the integral over the L_3 edge and q is the integral over the L_3 and L_3 edges.

Figure 3 shows XAS and XMCD data for the as-grown sample (a,b) and the annealed sample (c, d) at the Fe $L_{2,3}$ edges. The XAS at the Fe $L_{2,3}$ edges for both samples shows multiplet structure typical of iron oxide. Three peaks, two negative and one positive, are present in the XMCD spectra at the L_3 edge, similar to that found in other XMCD studies of Fe_3O_4 [13]. These peaks correspond to contributions from Fe^{3+} in octahedral (O_h), Fe^{3+} in tetrahedral (T_d) and Fe^{2+} in octahedral sites. For the ferrimagnetic spinel structure, spins located on the T_d sites are aligned antiparallel to the spins on the O_h sites [15]. Hence, the positive peak in the XMCD at the L_3 edge is due to tetrahedrally coordinated Fe^{3+}. Fits to the XMCD data using atomic multiplet calculations [16] show that the XMCD spectra for the as-grown sample is best represented by the ratio for the Fe^{2+} O_h, Fe^{3+} T_d and Fe^{3+} O_h of 0.8 : 1.05 :

1.05, whereas for the annealed sample a ratio of 1.05 : 1 : 0.95 is obtained. A clear increase in the amount of Fe^{2+} contributing to the magnetic signal is observed upon annealing the sample, consistent with the reducing CO/CO_2 environment and further demonstrating an improved stoichiometry of the film.

Integrating the XMCD spectra and applying the XMCD sum rules [,17] provides the spin to orbital magnetic moment ratio. In 3*d* transition metals the orbital magnetic moment is almost completely quenched by the crystal field interaction, and so the *g*-factor is approximately equal to the free-electron value of 2. For small orbital contributions, the *g*-factor can be expressed as [18]

$$g = 2\left(\frac{\mu_L}{\mu_S} + 1\right), \tag{1}$$

where μ_S and μ_L are the spin and orbital magnetic moment, respectively. The ratio of the orbital to spin magnetic moment can be conveniently obtained from the XMCD sum rules such that [13]

$$\frac{\mu_L}{\mu_S} = \frac{2q}{9p - 6q} \tag{2}$$

where *p* and *q* are the integrated intensities over the L_3 and $L_{2,3}$ XMCD signal, respectively. For the as-grown film we obtain $g = 2.14 \pm (0.01)$ whilst for the annealed film the XMCD sum rules give $g = 2.18 \pm (0.01)$. As can be seen directly from the integrated XMCD, this is due to a larger orbital moment ($\mu_L \propto q$) for the annealed film (0.27 μ_B) compared to the as-grown material, consistent with the increase in Fe^{2+} for the former.

A debate on the size of the orbital moment in Fe_3O_4 has been ongoing for the last 15 years. Goering *et al.* [19] measured a vanishingly small orbital moment whilst Huang *et al.* [20] measured a large orbital moment of 0.67 μ_B; both studies used high quality single crystals of Fe_3O_4. Artefacts due to self-absorption in TEY, the extent of the integration range in sum rule analysis and site compensation of orbital moments have all been invoked to explain the discrepancy [21]. More recently, quadrupole transitions at the *K*-edge XMCD of bulk Fe_3O_4 gave an orbital moment of 0.26 μ_B, associated with the formal Fe^{2+} site, in good agreement with our results [22]. The orbital magnetic moment was shown to have a strong dependence on the magnetic field direction leading to large variations in the measured magnitude, a possible explanation for the observed differences reported in the literature. One implication of a fully quenched orbital moment, as found by Goering *et al* [19], is that $g = 2$ which can easily be verified by FMR spectroscopy. Surprisingly, the data obtained from the two spectroscopic methods (XMCD and FMR) have not been extensively compared for this "model" ferrimagnetic oxide system. Bickford *et al.* [23] measured the *g*-factor in a number of bulk Fe_3O_4 samples using angle dependent FMR and obtained a *g*-factor of 2.12 and 2.17 for natural and synthetic samples respectively. The results of this seminal study strongly suggest a non-zero orbital moment in Fe_3O_4 and are in good agreement with the *g*-factor obtained by XMCD on the annealed thin film sample of this current study ($g = 2.18$) and in the recent *K*-edge data of bulk magnetite [22].

In order to obtain secondary evidence of a non-zero orbital moment via the *g*-factor, angle resolved FMR spectra were measured for the two samples. For these measurements, a broadband field modulated FMR was utilized in combination with an electromagnet capable of applying a field at any point in a circle of 0.5 T radius. The plane of the sample was aligned with the plane of rotation in order to measure the in-plane magnetic anisotropy.

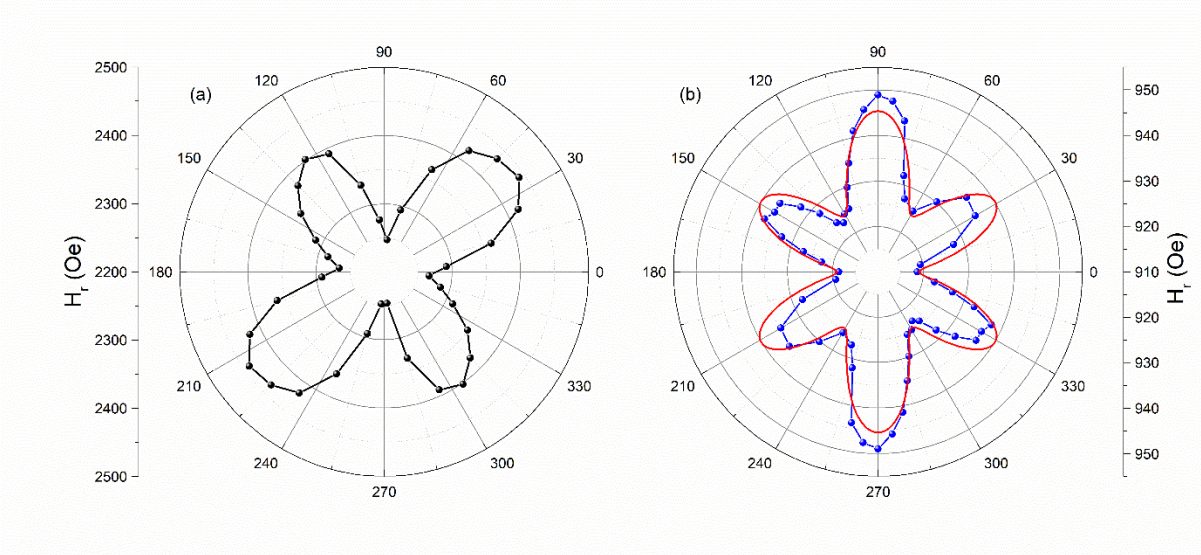

Figure 4: In plane (azimuthal) dependence of the FMR resonant field (H_r) measured at 10 GHz for (a) the as-grown film and (b) the film annealed at 1100 ℃. The red curve in (b) is a simulated curve generated using Eq. (4) and extracted parameters.

Field sweeps along different azimuthal angles at a fixed frequency were measured to observe changes in the resonance reflecting the in-plane anisotropy of the samples. Fig. 4 shows the in-plane anisotropy for the (a) as-grown and (b) annealed films respectively. The frequency of excitation was 10 GHz with the applied field (H) at $\phi = 0°$ corresponding to the $[1\bar{2}1]$ axis of the sample. The as-grown film displays a distorted fourfold symmetry whilst the annealed film shows a combination of six-fold and two fold symmetries. For the annealed film the measured anisotropy is predominantly cubic with the easy axis along $[1\bar{2}1]$. For cubic magnetic thin films grown on (111) surfaces the effective demagnetizing field forces the magnetic moment of the system to lie close to the (111) plane, perpendicular to the surface normal. The first-order magnetocrystalline anisotropy (MCA) is along the <111> directions for negative K_c, with the competition between the MCA and demagnetising field resulting in a small deviation of the magnetization away from the (111) plane. As a result, the in-plane resonance field should display six-fold symmetry with the in-plane easy axes along the $\langle 1\bar{2}1 \rangle$ directions for negative K_c. The cubic contribution to the measured anisotropy for a flat (111) film is small, with variations in the resonance field on the order of a few 10's Oe [24]. In-plane uniaxial anisotropy should not be present in a pure cubic system. However, a small in-plane uniaxial anisotropy is present in the annealed film as evidenced by the slightly lower resonance field along $[1\bar{2}1]$ compared to the other easy axis directions. Uniaxial anisotropies on cubic (111) surfaces have also been seen previously where thin films of Fe grown on Si(111) substrates have been shown to display a step edge induced uniaxial anisotropy [25].

The as-grown film shows an intriguing in-plane anisotropy. For a cubic system measured in the (001) plane a four-fold symmetry, similar to Fig. 4(a), would be expected; with easy axes along the [100] and [010] directions displaying resonant field minima. However, for films grown on YSZ(111) the anisotropy should be six-fold symmetric. Non-epitaxy with the substrate may relax this condition yet the XRD data gives evidence that the film is (111) orientated. There is no clear explanation for the observed angular dependence of the magnetic resonance although, speculatively, this may be a consequence of a small miscut of the substrate leading to a high step edge density and mosaicity of the film. As reported in Ref. [25] small misorientations are sufficient to reduce the six-fold symmetry to a four-fold one, resulting in variations in the resonant field much larger than in the (111) plane, which is what we observe experimentally. Annealing at high temperatures (1100°C) may smooth the interface, reducing the mosaicity and allowing for a recovery of the six-fold symmetry. We also note

that the diffraction intensity of the (*hhh*) Fe_3O_4 reflections are higher after annealing, supporting this hypothesis.

Values of the *g*-factor were obtained by measuring FMR field swept spectra as a function of RF driving frequency in the range 4 – 20 GHz. FMR ideally measures the imaginary part of the complex magnetic susceptibility which is best represented by a symmetric Lorentzian lineshape. However, FMR line shapes are often asymmetric due to a small mixing of the real and imaginary parts of the magnetic susceptibility [26]. In our FMR absorption measurements *H* is modulated so that the measured signal can be represented by the derivative of the asymmetric Lorentzian with respect to *H* such that

$$\frac{dP}{dH} = C\frac{-(H-H_R)\Delta H\cos\varepsilon - [(\Delta H/2)^2 - (H-H_R)^2]\sin\varepsilon}{[(\Delta H/2)^2 + (H-H_R)^2]^2} \quad (3)$$

where *C* is a constant, *H* is the applied field, H_R is the resonant field, $\Delta H/2$ is the linewidth corresponding to the HWHM of the Lorentzian and ε is the phase that mixes real and imaginary parts of the susceptibility. For $\varepsilon = 0°$ the line shape is purely due to the imaginary part of the susceptibility. The experimental data (symbols) in Fig. 4(a), measured at 10 GHz, is fitted using Eq. (3) (lines). For both films $\varepsilon \approx 0°$. Resonance for the as-grown film occurs at a bias field of 2370 Oe and displays a relatively large linewidth ΔH, defined as the peak to peak width multiplied by $\sqrt{3}/2$, of 1060 Oe. The annealed film shows a stronger resonant amplitude (≈ 30x), a resonance at a lower bias field, 920 Oe, and a narrower linewidth ($\Delta H \approx$ 230 Oe). The reduction in both the resonance field and linewidth correlate to an improved magnetic structure. Resonant fields were extracted for each driving frequency and are plotted in Fig. 5(b) for the as-grown and annealed films.

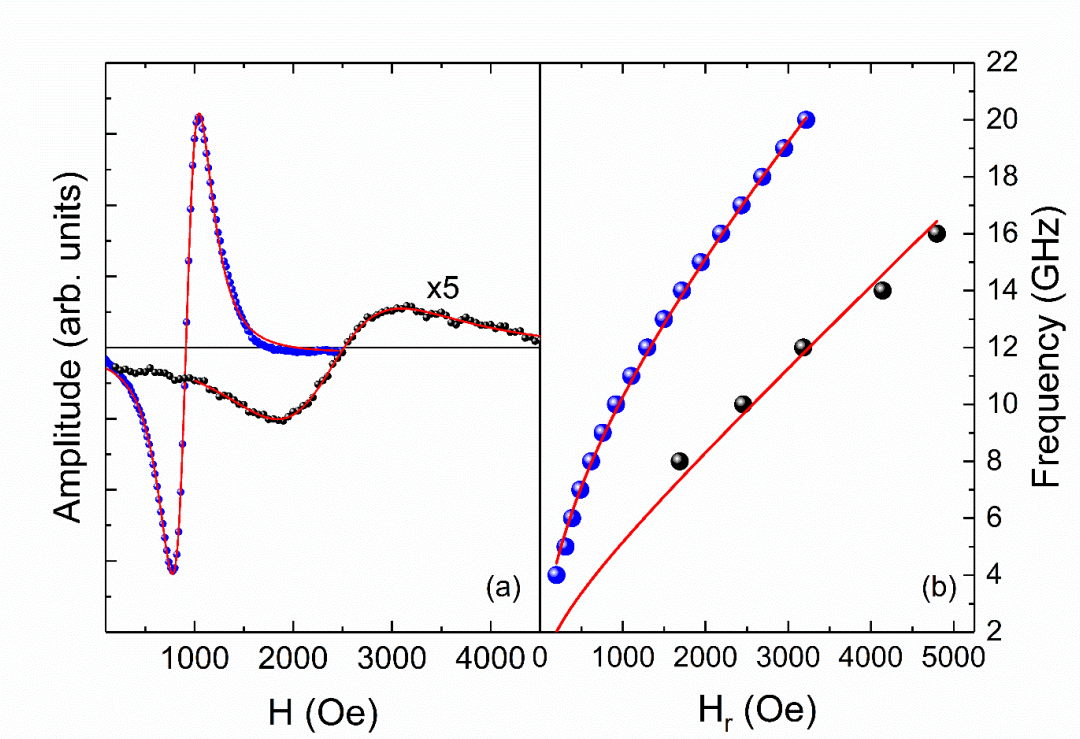

Figure 5: (a) FMR absorption measurement at 10 GHz for the as-grown (black data points) and annealed (blue) films. (b) Kittel curves (frequency vs resonant field) for the as-grown (black) and annealed films (blue).

The data for the annealed sample was fitted using the Kittel equation [27] for a (111) surface and applied fields along the easy axis ($\phi = 0°$),

$$f = \frac{\gamma}{2\pi}\left[\left(H + 2\frac{K_{u||}}{M}\cos(2\phi)\right)\left(H - \frac{K_1}{M} + \frac{K_{u||}}{M}(1+\cos(2\phi)) + 4\pi M_{eff}\right) - 2\frac{K_1^2}{M^2}\sin^2(3\phi)\right]^{1/2} \quad (4)$$

where K_1 and $K_{u||}$ are the bulk cubic and in-plane uniaxial magnetocrystalline anisotropy constants respectively, ϕ is the azimuthal angle (in-plane) between the magnetization (field) direction and the anisotropy axis (which is simplified as both K_1 and $K_{u||}$ have a common axis), and $4\pi M_{\text{eff}} = 4\pi M - 2K_{u\perp}/M$ where $K_{u\perp}$ is the out of plane uniaxial anisotropy constant. The *g*-factor is obtained via the definition of the gyromagnetic ratio $\gamma = ge/2m$. For the annealed film a *g*-factor of 2.19 ± 0.01 is obtained; in good agreement with the value obtained via XMCD and in Ref. [22]. Fits to the FMR data for the annealed film give a large out of plane uniaxial anisotropy constant (-8.8 x 10^5 erg/cc). Such a large anisotropy has been reported before [28,29], but the physical origin not determined. We provide evidence that such a large perpendicular anisotropy is magnetoelastic in origin. The magnetoelastic contribution to the magnetic free energy along the [111] direction is given by,

$$f_{ME} = 3\lambda_{111}c_{44}\varepsilon_{111}\sin^2\theta = K_{ME}\sin^2\theta$$

where λ_{111} is the saturation magnetostriction along the <111> directions, c_{44} the relevant elastic constant, ε_{111} the strain along the out of plane [111] axis and θ the angle the magnetization makes with the strain axis. From the literature, we obtain $\lambda_{111} \approx 90 \times 10^{-6}$ and $c_{44} \approx 7 \times 10^{11}$ dyne/cm^2 [30, 31] for Fe_3O_4. From the XRD data we measure a strain of -0.49% in the out of plane direction for the annealed sample which then gives $K_{ME} = -9.3 \times 10^5$ erg/cc; close to the value extracted from the fits to the FMR data for $K_{u\perp}$. Using the extracted values for the anisotropy constants, magnetization, *g*-factor and Eq. (4) we generate the in-plane resonance field for a fixed frequency of 10 GHz which is plotted as the solid line in Fig. 4(b). As can be seen, the simulated curve is in good agreement with the experimental data indicating we have captured all the pertinent contributions to the magnetic free energy density. Fits to the frequency field data for the as-grown sample have been performed assuming a cubic-like free energy with the [001] axis perpendicular to the film plane; in contradiction to the XRD data. Therefore, we do not provide details of the fitting parameters as our free energy model is inaccurate. However, from the experimental data we observe that the *g*-factor is reduced compared to the annealed film, consistent with the XMCD.

We note that Kittel's original derivation of the spectroscopic *g*-factor (Eq. (1)) [18] may require modification as to include the spin mixing of the valence band states [32]. Shaw *et al.* [32] demonstrated a discrepancy between the *g*-factor obtained from FMR and XMCD for a CoFe/Ni multilayer and Py film which they account for by including the second-order spin mixing parameter, b^2, in Eq. (1). Whilst the authors note a large difference in the uncorrected ratio of the orbital to spin moment as measured by FMR and XMCD for Ni, the difference between the two techniques for the uncorrected moment ratio of Fe is much smaller, suggesting a reduced spin mixing parameter. As the spin-mixing parameter is a consequence of spin-orbit coupling, the effect will be also be minimized in materials containing d^5 ions [33]. We therefore expect that the correction to the *g*-factor due to second-order spin-mixing terms to be small for Fe_3O_4, and well within our experimental uncertainty. Therefore, we do not include such effects in the analysis.

From the static magnetic data, it is evident that annealing the sample in CO/CO_2 has improved the magnetic properties of the Fe_3O_4 thin films. Intuitively we would therefore also expect that the

dynamic properties of the film, such as the magnetic damping, to also be improved commensurately. However, care must be taken; the larger orbital moment of the annealed film may give rise to enhanced Gilbert damping, as was shown by Hrabec *et al.* [34]. Complementary to obtaining the resonant fields as a function of frequency, fits to the field swept FMR data enable the frequency dependent linewidth (ΔH) to be extracted. Fig. 6 shows the field linewidth vs frequency for the as-grown and annealed samples respectively.

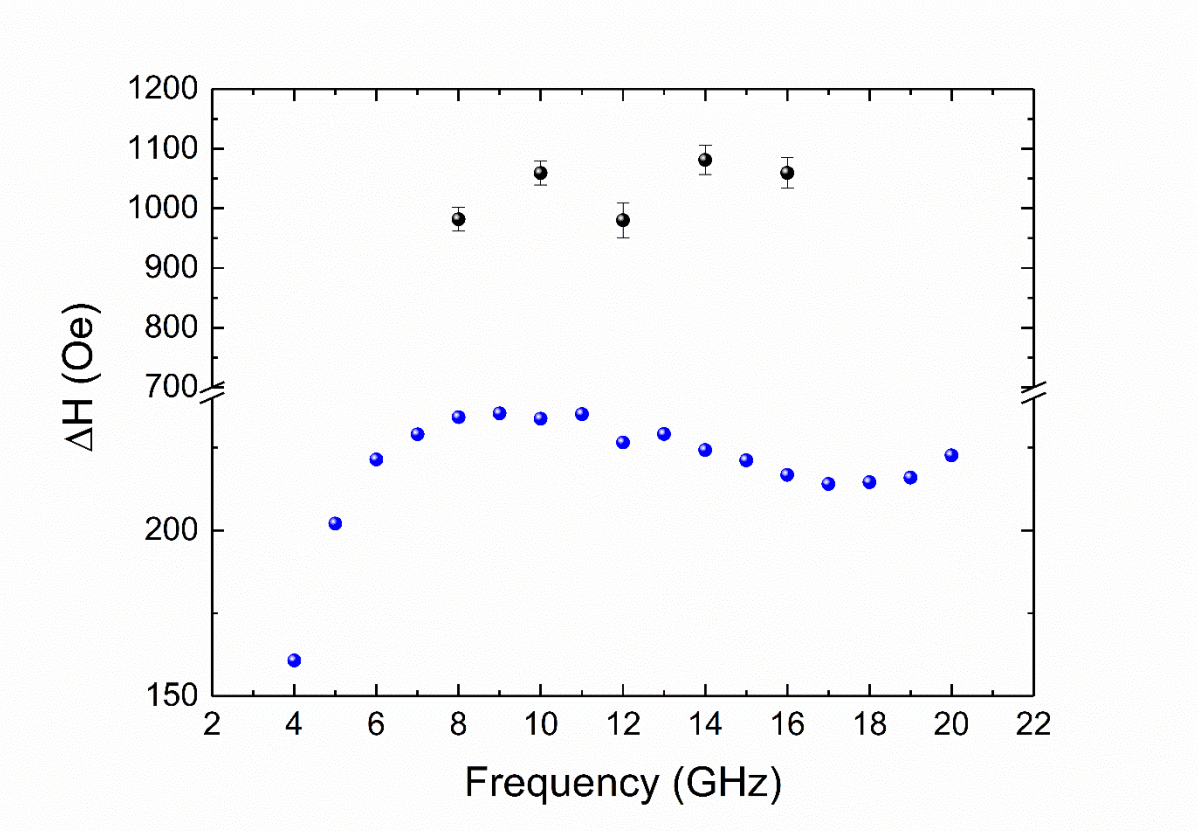

Figure 6: FMR linewidth (ΔH) vs frequency for the as-grown (black) and annealed (blue) Fe_3O_4 films.

For the as-grown sample, the linewidth is broad (≈ 1000 Oe) and relatively insensitive to frequency. Due to the broad linewidth, data could not be obtained below an FMR frequency of 8 GHz. The flat response of ΔH to frequency is indicative of extrinsic damping due to magnetic inhomogeneities or mixed magnetic phases within the sample. The field linewidth is attributed to a summation of broadening mechanisms [35]

$$\Delta H = \Delta H_0 + \Delta H_{\mathrm{TMS}} + \Delta H_{\mathrm{int}} = \Delta H_0 + \Delta H_{\mathrm{TMS}} + \frac{2\pi\alpha}{\gamma} f \tag{5}$$

where f is the microwave frequency, and α is the dimensionless Gilbert damping parameter. The different frequency dependence of these contributions allows for determination of the dominant relaxation mechanism in the sample. While the intrinsic Gilbert damping (ΔH_{int}) shows a linear frequency dependence, magnetic inhomogeneities can lead to a linewidth offset (ΔH_0) and two magnon scattering (ΔH_{TMS}). Two magnon scattering contributions scales non-linearly with microwave frequency, saturating at high frequencies and presenting a steep increase at lower frequencies [36].

The resulting FMR linewidth (ΔH) is the sum of these contributions. For the annealed sample the linewidth vs frequency data shows a characteristic two-magnon scattering line shape again indicating magnetic inhomogeneities, or mixed magnetic phases, within the sample but with a much reduced linewidth compared to the as-grown sample. However, after the steep increase at low frequencies the linewidth not only levels off at higher frequencies but decreases slightly before again increasing after 17 GHz. The consequence of this is a broad peak in $\Delta H(f)$. This profile is not expected from a simplistic view of magnetic relaxation in which the linewidth should always increase with frequency, as shown in Eq. (5). Such a profile is observed in spherical samples in which the "Buffler" peak [37], due to the band-edge crossover effect, is the signature for grain-to-grain two-magnon scattering. The Buffler peak is a purely geometric effect that although is present in spherical samples, should not be observed in thin films. Landeros *et al.* [38] show a similar feature in calculations of the FMR linewidth due to two-magnon scattering when there is a small tipping angle ($\approx 5°$) between the magnetization and film plane. The non-monotonic behaviour of the linewidth with frequency at these angles is similar in shape to our experimental data. In [38] the angle is kept constant as a function of frequency, which is not possible experimentally due to the increasing in-plane H field with frequency. However, this would smooth out the effect for modest changes in the polar angle of the magnetization and the effect is visible over a broad range of polar angles. Only when M is exactly in-plane does the linewidth with frequency show monotonic behaviour. Calculating the magnetic free energy density (F) for the (111) orientation of Fe_3O_4 including the magnetocrystalline anisotropy energy, demagnetization energy and Zeeman energy for an in-plane field of 1000 Oe ($\theta_H = 90°$, $\phi_H = 180°$), we find that the free energy is minimized ($\partial F/\partial\theta = 0$, $\partial F/\partial\phi = 0$) when the magnetization is tilted marginally out of plane by $\approx 2°$ as shown in Fig. 7.

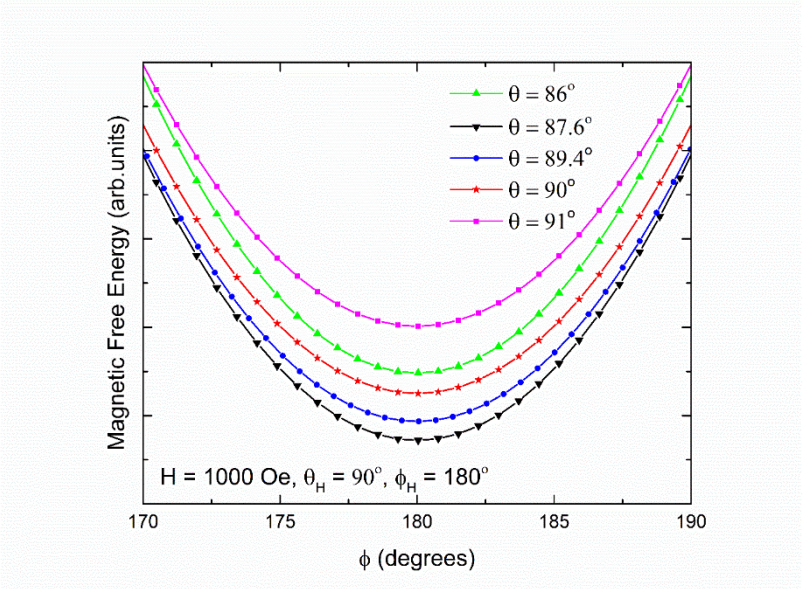

Figure 7: Magnetic free energy density plotted as a function of the polar (θ) and azimuthal angle (ϕ) for Fe_3O_4.

According to Ref. [38], this small tilting angle would give rise to the observed non-monotonic behaviour in the FMR linewidth with frequency consistent with our data.

Summary
Thin film Fe_3O_4 was grown on YSZ(111) substrates using PLD. High temperature (1100 °C) annealing in a reducing atmosphere allows bulk-like structural and magnetic properties to be recovered without significant film substrate intermixing. An unusual four-fold magnetic anisotropy is observed for the as-grown films that transforms to the expected six-fold symmetry of the (111) surface upon annealing. A finite orbital moment was measured using XMCD and FMR, in agreement with recent hard x-ray measurements, adding further evidence to a long standing and contentious debate concerning this quantity. Whilst bulk-like static magnetic properties are recovered upon annealing, the high frequency dynamic properties are still dominated by two-magnon scattering and a non-monotonic behavior observed in field linewidth as a function of frequency in agreement with the predictions of Landeros *et al.* [38].

Acknowledgements
The authors acknowledge the Diamond Light Source for beamtime on beamline I06 under SI14135.

[1] C. Fesler, G. H. Fecher and B. Balke. Angew. Chem., **46**, 668 (2007)
[2] W. Eerenstein, T. T. M. Palstra, S. S. Saxena, and T. Hibma, Phys. Rev. Lett. **88**, 247204 (2002).
[3] Keith P. McKenna, Florian Hofer, Daniel Gilks, Vlado K. Lazarov, Chunlin Chen, Zhongchang Wang & Yuichi Ikuhara. Nat. Comms **5**, 5740 (2014)
[4] J. B. Goodenough. J. Phys. Chem. Solids, **6**, 287 (1958). J. Kanamori. J. Phys. Chem. Solids, **10**, 87 (1959).
[5] W. Erenstein, T. T. M. Palstra, T. Hibna and S. Celotto. Phys. Rev. B **66**, 201101 (R) (2002)
[6] E. Liu, Y. Yin, L. Sun, Y. Zhai, J. Du, F. Xu and H. Zhai. Appl. Phys. Lett. **110**, 142402 (2017)
[7] D. Gilks, L. Lari, K. Matsuzaki, H. Hosono, T. Susaki, and V. K. Lazarov. J. Appl. Phys. **115**, 17C107 (2014)
[8] S. S. Kalarickal, N. Mo, P. Kivosik and C. E. Patton. Phys. Rev. B **79**, 094427 (2009)
[9] C. J. Love, B. Kuerbanjiang, A. Kerrigan, S. Yamada, K. Hamaya, G. van der Laan, V. K. Lazarov, and S. A. Cavill. Appl. Phys. Lett. **119**, 172404 (2021)
[10] Balati Kuerbanjiang, Christopher Love, Demie Kepaptsoglou, Zlatko Nedelkoski, Shinya Yamada, Arsham Ghasemi, Quentin M. Ramasse, Kohei Hamaya, Stuart A. Cavill, Vlado K. Lazarov. Journal of alloys and compounds **748**, 323 (2018)
[11] S. S. Dhesi, S. A. Cavill, A. Potenza, H. Marchetto, R. A. Mott, P. Steadman, A. Peach, E. L. Shepherd, X. Ren, U. H. Wagner, and R. Reininger. AIP Conference Proceedings, **1234**, 311 (2010)
[12] E.J. Verwey, Nature (London) **144**, 327 (1939); X.Liu, C-F. Chang, A. D. Rata, A. C. Komarek and L. H. Tjeng. Npj Quantum Materials **1**, 16027 (2016)
[13] G. van der Laan and A. I. Figueroa. Coord. Chem. Rev **95**, 277 (2014)
[14] R. Nakajima, J. Stohr and Y. U. Idzerda. Phys. Rev. B. **59**, 6421 (1999)
[15] P. Morrall, F. Schedin, G. S. Case, M. F. Thomas, E. Dudzik, G. van der Laan, and G. Thornton. Phys. Rev. B **67**, 214408 (2003)
[16] G. van der Laan and B. T. Thole, Phys. Rev. B **43**, 13401 (1991), E. Stavitski and F. M. F. de Groot. Micron, **41**, 687 (2010)
[17] B.T. Thole, P. Carra, F. Sette and G. van der Laan, Phys. Rev. Lett. **68**, 1943 (1992); C. T. Chen, Y. U. Idzerda, H.-J. Lin, N. V. Smith, G. Meigs, E. Chaban, G. H. Ho, E. Pellegrin, and F. Sette. Phys. Rev. Lett. **75**, 152 (1995)
[18] C. Kittel. Phys. Rev. **6**, 743 (1949)
[19] E. Goering, S. Gold, M. Lafkioti and G. Schutz. EPL **73**, 97 (2005)
[20] D. J. Huang, C. F. Chang, H.-T. Jeng, G. Y. Guo, H.-J. Lin, W. B. Wu, H. C. Ku, A. Fujimori, Y. Takahashi, and C. T. Chen. Phys. Rev. Lett. **93**, 077204 (2004)
[21] E. Goering. Phys. Status Solidi B 248, 2345 (2011)

[22] H. Elnaggar, Ph. Sainctavit, A. Juhin, S. Lafuerza, F. Wilhelm, A. Rogalev, M.-A. Arrio, Ch. Brouder, M. van der Linden, Z. Kakol, M. Sikora, M. W. Haverkort, P. Glatzel, and F. M. F. de Groot. Phys. Rev. Lett. **123**, 207201 (2019)
[23] L. R. Bickford. Phys. Rev. **78**, 449 (1950)
[24] C. J. Love, B. Kuerbanjiang, A. Kerrigan, S. Yamada, K. Hamaya, G. van der Laan, V. K. Lazarov, and S. A. Cavill. Appl. Phys. Lett. **119**, 172404 (2021)
[25] H-F. Du, W. He, H-L. Liu, Y-P. Fang, Q. Wu, T. Zou, X-Q. Zhang, Y. Sun and Z-H. Cheng. APL **96**, 142511 (2010)
[26] D. E. Parkes, L. R. Shelford, P. Wadley, V. Holý, M. Wang, A. T. Hindmarch, G. van der Laan, R. P. Campion, K. W. Edmonds, S. A. Cavill & A. W. Rushforth. Sci. Reports **3**, 2220 (2013)
[27] J. Smit and H. G. Beljers, Philips Res. Rep. **10**, 113 (1955). G. Gubbiotti *et al*. J. Phys.: Condens. Matter **10**, 2171 (1998)
[28] Y. Zhai, Z. C. Huang, Y. Fu, C. Ni, Y. X. Lu, Y. B. Xu, J. Wu and H. R. Zhai. J. Appl. Phys. **101**, 09D126 (2007)
[29] Z. C. Huang, X. F. Hu, Y. X. Xu, Y. Zhai, Y. B. Xu, J. Wu, and H. R. Zhai. J. Appl. Phys. **111**, 07C108 (2012)
[30] L. R. Bickford, J. Pappis and J. L. Stull. Phys. Rev. **99**, 15, 1210 (1955)
[31] T. J. Moran and B. Luth. Phys. Rev. **187**, 710 (1969)
[32] J. M. Shaw, R. Knut, A. Armstrong, S. Bhandary, Y. Kvashnin, D. Thonig, E. K. Delczeg-Czirjak, O. Karis, T. J. Silva, E. Weschke, H. T. Nembach, O. Eriksson, and D. A. Arena. Phys. Rev. Lett. **127**, 207201 (2021)
[33] D. Cheshire, P. Bencok, D. Gianolio, G. Cibin, V. K. Lazarov, G. van der Laan and S. A. Cavill. J. Appl. Phys. **132**, 103902 (2022)
[34] A. Hrabec, F. J. T. Gonçalves, C. S. Spencer, E. Arenholz, A. T. N'Diaye, R. L. Stamps, and Christopher H. Marrows. Phys. Rev. B **93**, 014432 (2016)
[35] G. Woltersdorf and B. Heinrich. Phys. Rev. B **69**, 184417 (2004)
[36] R. Arias and D. L. Mills. Phys. Rev. B **60**, 7395 (1999)
[37] C. R. Buffler. J. Appl. Phys. **30**, S172 (1959)
[38] P. Landeros, R. E. Arias and D. L. Mills. Phys. Rev. B **77**, 214405 (2008)

Figure Captions

Figure 8: XRD measured in the symmetric geometry for (a) the as-grown sample and (b) the anenaled sample. Red arrows indicate the position of the (hhh) Fe_3O_4 reflections.

Figure 9: (a) M-H and (b) M-T for the as-grown film. (c) M-H and (d) M-T for the annealed film. M-H curves were measured at 300 K. M-T curves were measured after field cooling at 30 KOe. The measuring field was set to 1000 Oe.

Figure 10. Circular polarization dependent XAS at the Fe $L_{2,3}$ edges for (a) the as-grown sample and (c) the annealed sample. XMCD (blue dots) and integrated XMCD (green line) specta for (b) the as-grown sample and (d) the annealed sample. Atomic multiplet simulations of the XMCD are shown in red dash-dot line on top of the experimental XMCD. p is the integral over the L_3 edge and q is the integral over the L_3 and L_3 edges.

Figure 11: In plane (azimuthal) dependence of the FMR resonant field (H_r) measured at 10 GHz for (a) the as-grown film and (b) the film annealed at 1100 ℃. The red curve in (b) is a simulated curve generated using Eq. (4) and extracted parameters.

Figure 12: (a) FMR absorption measurement at 10 GHz for the as-grown (black data points) and annealed (blue) films. (b) Kittel curves (frequency vs resonant field) for the as-grown (black) and annealed films (blue).

Figure 13: FMR linewidth (ΔH) vs frequency for the as-grown (black) and annealed (blue) Fe_3O_4 films.

Figure 14: Magnetic free energy density plotted as a function of the polar (θ) and azimuthal angle (ϕ) for Fe_3O_4.

Figure. 1

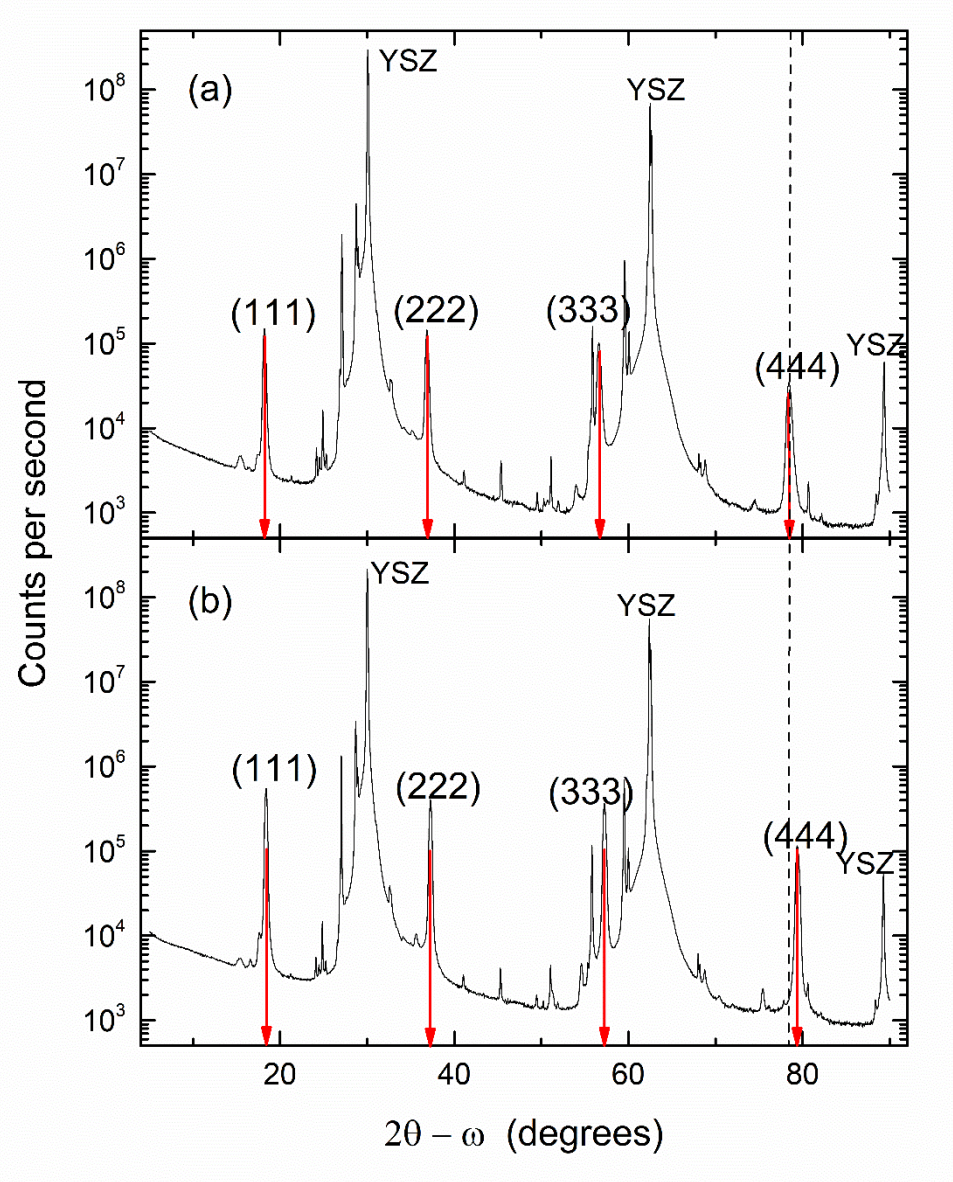
(a)
(b)
YSZ
(111)
(222)
(333)
(444)
Counts per second
2θ – ω (degrees)
10^8
10^7
10^6
10^5
10^4
10^3
20
40
60
80

Figure. 2

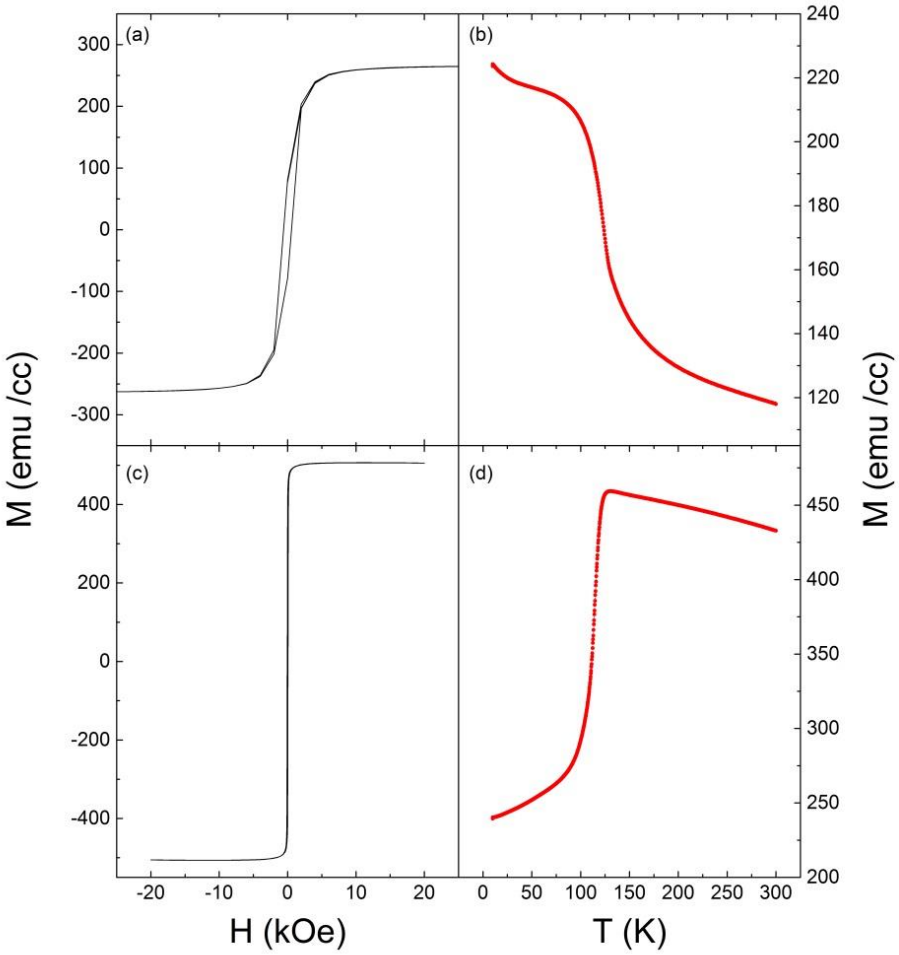
(a)
(b)
(c)
(d)
M (emu /cc)
M (emu /cc)
H (kOe)
T (K)
300
200
100
0
-100
-200
-300
240
220
200
180
160
140
120
400
200
0
-200
-400
450
400
350
300
250
200
-20
-10
0
10
20
0
50
100
150
200
250
300

Figure. 3

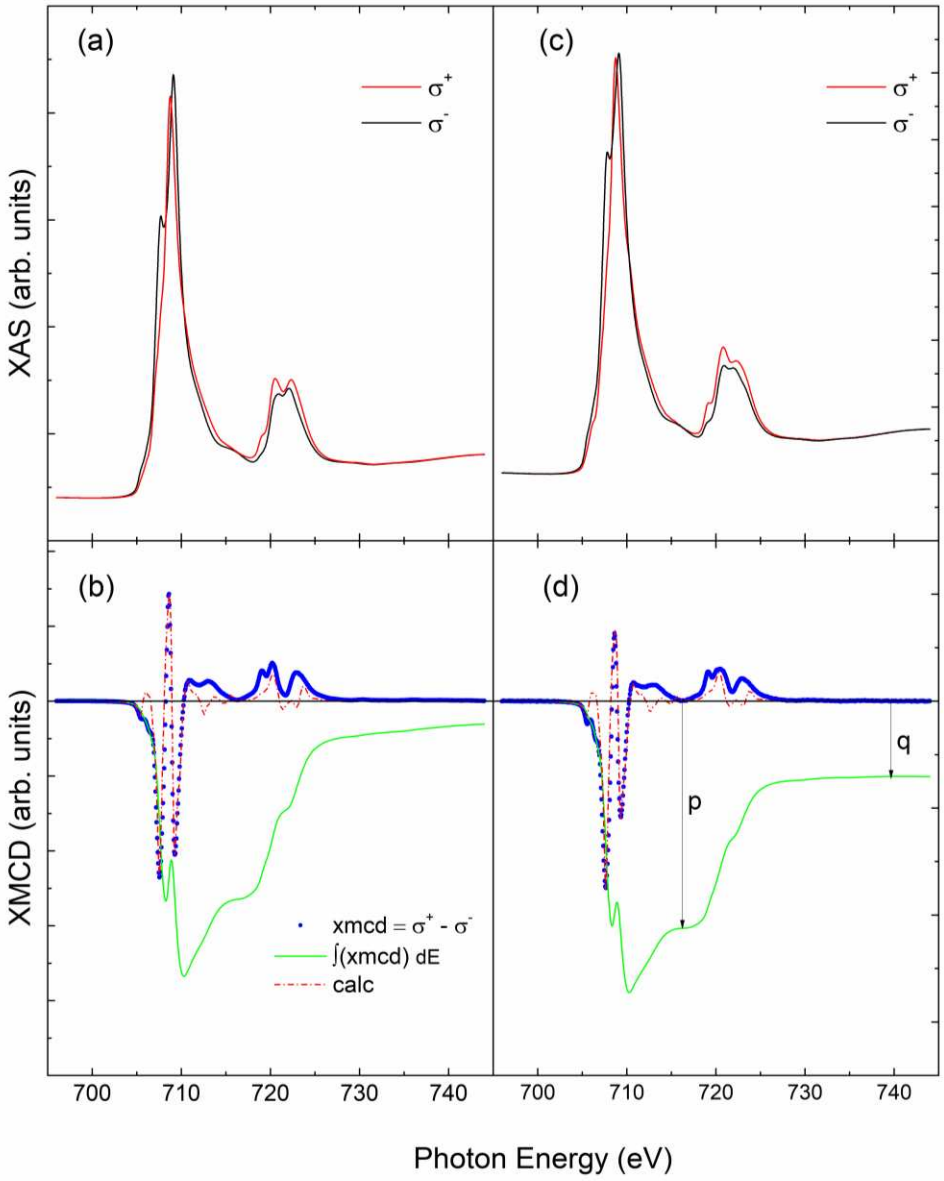
(a)
(c)
(b)
(d)
σ+
σ-
XAS (arb. units)
XMCD (arb. units)
xmcd = σ+ - σ-
∫(xmcd) dE
calc
p
q
700
710
720
730
740
Photon Energy (eV)

Figure. 4

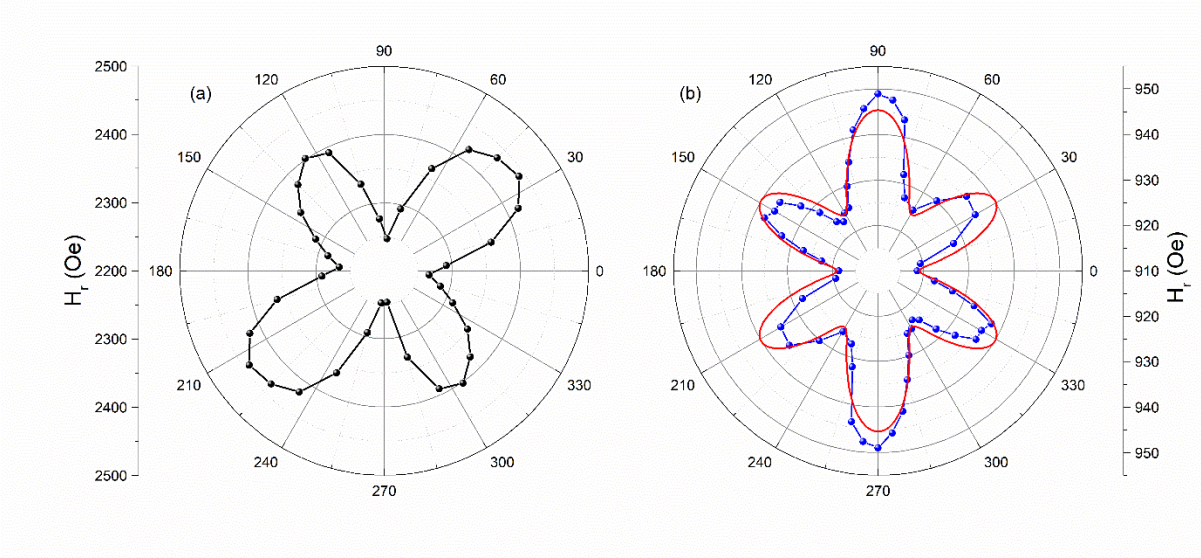
(a)
(b)
90
120
60
150
30
180
0
210
330
240
300
270
2500
2400
2300
2200
2300
2400
2500
H_r (Oe)
950
940
930
920
910
920
930
940
950
H_r (Oe)

Figure. 5

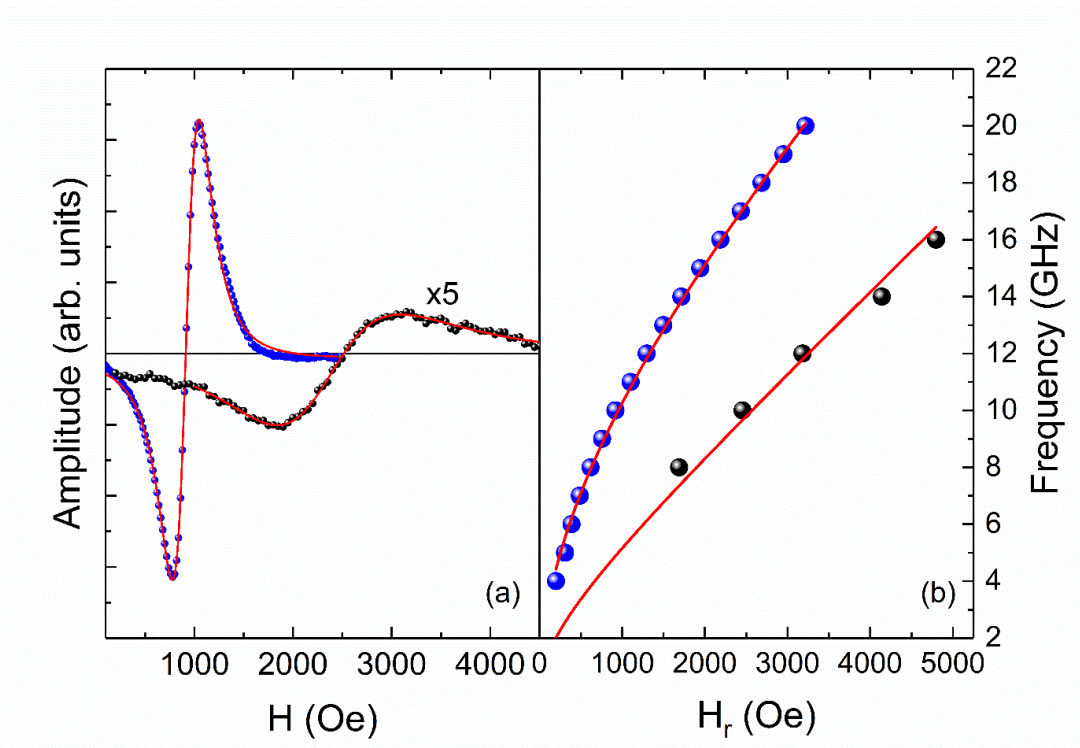
Amplitude (arb. units)
x5
(a)
1000
2000
3000
4000
H (Oe)
0
1000
2000
3000
4000
5000
H_r (Oe)
(b)
Frequency (GHz)
2
4
6
8
10
12
14
16
18
20
22

Figure. 6

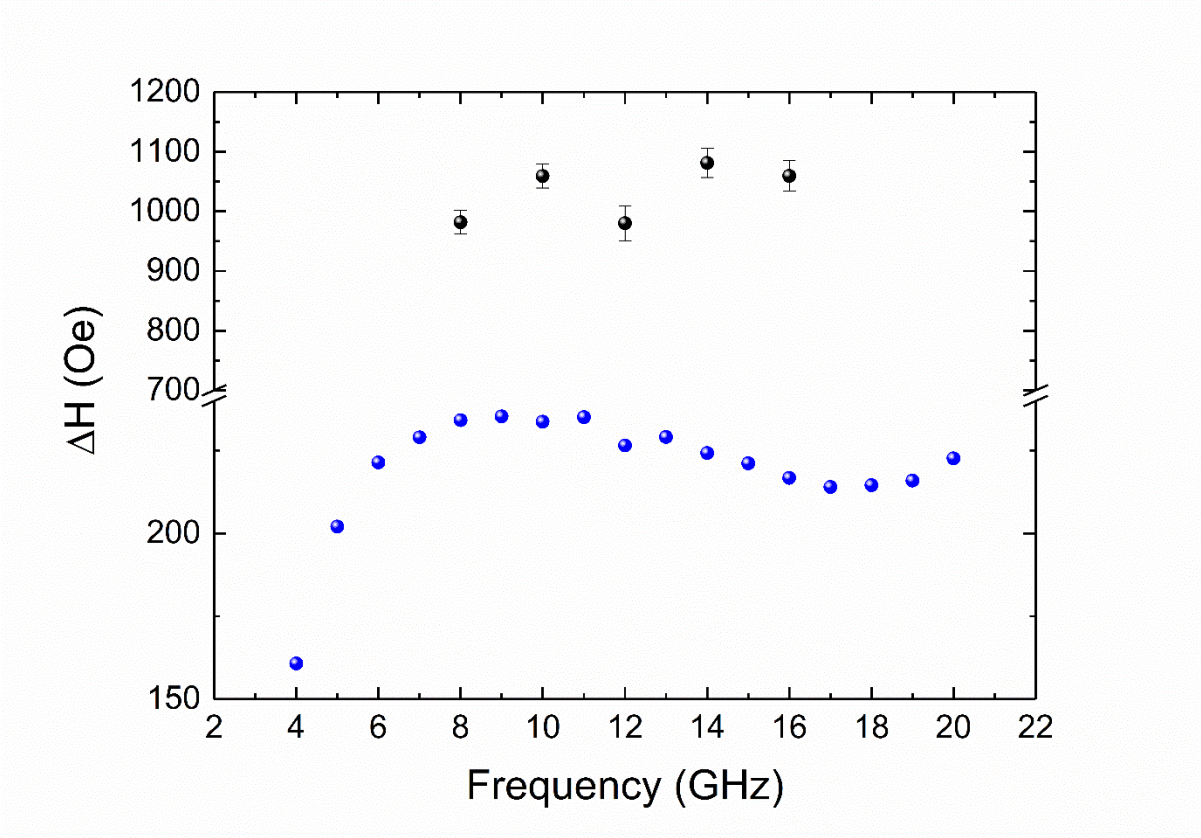
1200
1100
1000
900
800
700
200
150
ΔH (Oe)
2
4
6
8
10
12
14
16
18
20
22
Frequency (GHz)

Figure. 7

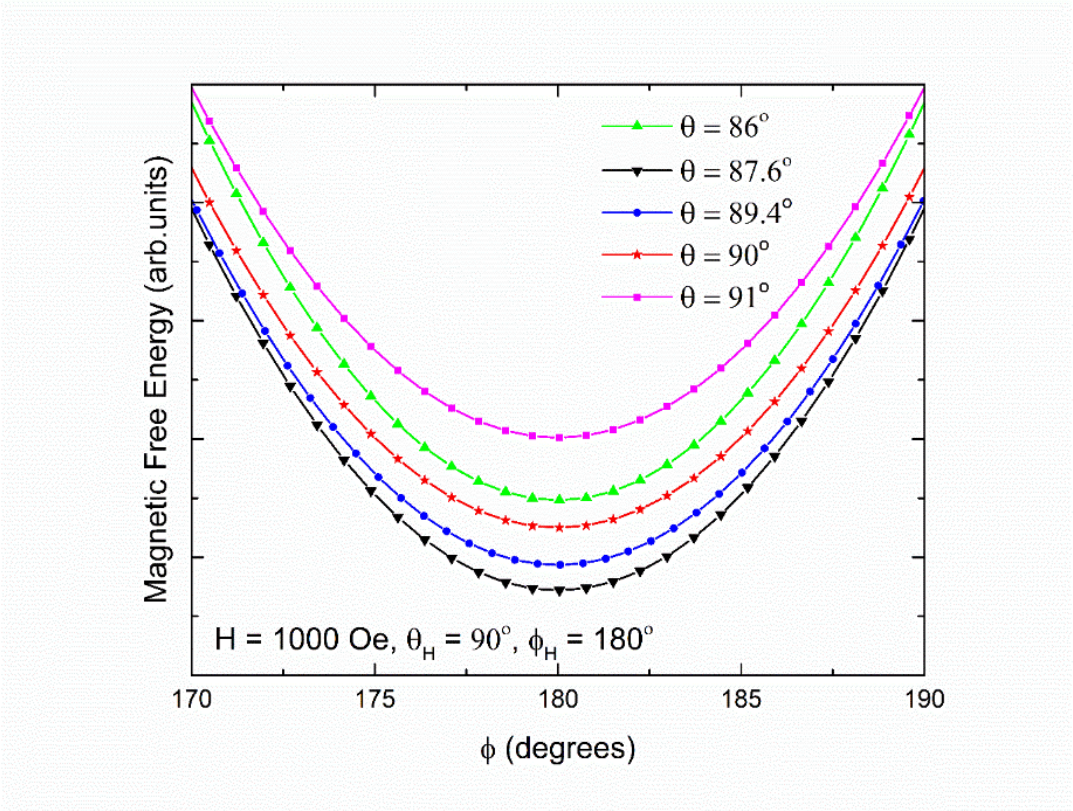
θ = 86°
θ = 87.6°
θ = 89.4°
θ = 90°
θ = 91°
H = 1000 Oe, θH = 90°, ϕH = 180°
Magnetic Free Energy (arb.units)
170
175
180
185
190
ϕ (degrees)